RESEARCH ARTICLE | JANUARY 05 2023

Morphed inception of dynamic Leidenfrost regime in colloidal dispersion droplets

Gudlavalleti V V S Vara Prasad ; Mohit Yadav; Purbarun Dhar ; Devranjan Samanta

Physics of Fluids 35, 012107 (2023)
https://doi.org/10.1063/5.0131609

Physics of Fluids ARTICLE scitation.org/journal/phf

Morphed inception of dynamic Leidenfrost regime in colloidal dispersion droplets

Cite as: Phys. Fluids **35**, 012107 (2023); doi: 10.1063/5.0131609
Submitted: 22 October 2022 · Accepted: 7 December 2022 ·
Published Online: 5 January 2023

Gudlavalleti V V S Vara Prasad,[1] Mohit Yadav,[1] Purbarun Dhar,[2,a)] and Devranjan Samanta[1,a)]

AFFILIATIONS

[1]Department of Mechanical Engineering, Indian Institute of Technology Ropar, Ropar, Punjab 140001, India
[2]Hydrodynamics and Thermal Multiphysics Lab (HTML), Department of Mechanical Engineering, Indian Institute of Technology Kharagpur, Kharagpur, West Bengal 721302, India

[a)]**Authors to whom correspondence should be addressed:** purbarun@mech.iitkgp.ac.in. **Tel.:** +91-3222-28-2938 and devranjan.samanta@iitrpr.ac.in. **Tel.:** +91-1881-24-2109

ABSTRACT

Droplet impact on a heated substrate is an important area of study in spray cooling applications. On substrates significantly hotter than the saturation temperature, droplets immediately hover on its vapor cushion, exhibiting the Leidenfrost phenomenon. Here, we report the phenomena wherein addition of Al_2O_3 nanoparticles to water significantly increases the onset of dynamic Leidenfrost temperature (T_{DL}) and suppresses the overall Leidenfrost regime. We experimentally revealed that the onset of T_{DL} delays with increasing the nanoparticle concentration of the colloidal dispersions at a particular Weber number (We). But, for a constant concentration, the onset of T_{DL} decreases with an increase in impact We. In contrast to water droplets, the colloid droplets exhibit vigorous spraying behavior due to the nanoparticulate residue deposition during the spreading and retraction stages. Further, the residue on the heated substrate changes the departure diameter of the vapor bubbles during boiling, prevents bubble coalescence and vapor layer formation, and reduces the propensity to attain dynamic Leidenfrost regime. With the aid of scaling analysis of T_{DL} with impact We, we have explored the thermo-hydrodynamic behavior of impacting colloid droplets on a superheated substrate. Finally, we have also segregated the different boiling regimes of colloid droplets over various impact We.

I. INTRODUCTION

When a droplet is deposited on a surface heated at temperatures much higher than the liquid's boiling point, the droplet levitates on its own vapor cushion, and this is known as the Leidenfrost effect.[1] Droplet impact on superheated surfaces finds direct implications toward utilities in various domains, like spray cooling,[2] fire suppression,[3] electronics cooling,[4] material quenching,[5] cooling of nuclear fuel rods,[6] and so forth. The thin, micrometer-scale vapor layer acts as a thermal insulator at the solid–liquid interface and significantly affects the heat transfer from the heated substrate to the fluid droplet. At the same time, it propels the droplet away from the surface via intermittent levitation. Hence, often it is desirable to delay the onset of the Leidenfrost effect for better thermal management of overheated components.

Researchers have explored in various directions and targeted to increase the Leidenfrost point by different techniques, viz., the addition of nanoparticles,[7,8] polymers,[9,10] surfactants,[11,12] nanobubbles,[13] and use of an external electric field.[14] Duursma *et al.*[7] tested the efficacy of nanoparticle solutions in spray cooling. For DMSO (dimethyl sulfoxide) nanofluids, they observed a significant enhancement of heat flux compared to water. In addition, they noticed a decrease in drop breakup during the retraction phase and maximum spreading diameter. Similarly, Paul *et al.*[8] observed an increase in the Leidenfrost point using an aqueous solution of TiO_2 nanoparticles. Due to the nanoparticle deposition, stable vapor layer formation is disrupted leading to a delay in attaining the Leidenfrost state. Bertola observed and reported the behavior of polymeric non-Newtonian fluid droplets and the shift of the Leidenfrost point.[9]

Dhar *et al.* showed the behavior of polymeric droplets during the droplet's retraction phase and the effect of threshold impact velocity and polymer concentration on the increase in the Leidenfrost point.[10] Chen *et al.*[11] showed that the addition of high alcohol surfactants (HASs) like 1-octanol and 2-ethyl-hexanol alcoholic surfactant droplets delay the Leidenfrost point. They hypothesized that due to a reduction in surface tension, the droplets attain greater spreading diameter with a thinner liquid disk. In the case of a thinner liquid disk,

it is easier for the vapor bubbles to burst out from the drop and disrupt the Leidenfrost state. Also, lower surface tension implies lower bubble departure and subsequent delay in bubble coalescence and vapor layer formation. Prasad *et al.*[12] achieved a delay in the T_{DL} by adding anionic and cationic surfactants to water droplets. They invoked the role of dynamic surface tension on the maximum spread factor during the Leidenfrost stage. They reported the effect of Taylor–Marangoni instability on the shift of T_{DL} with various surfactant concentrations at a fixed *We*. They have also revealed the effect of novel thermohydrodynamic events like Trampoline and Jetting dynamics during droplet impact on superheated surfaces. Later, Prasad *et al.*[13] introduced a novel methodology of oxygen nanobubbles dispersed droplets for the augmentation of dynamic Leidenfrost point. They discussed the effect of the constant contact radius (CCR) mode of contact boiling stage for different nanobubble concentrations with various *We*. Contrary to the intuition that presence of nanobubble will promote the early onset of the Leidenfrost state, this study showed the delay in vapor layer formation and enhancement of T_{DL}.[13]

In addition, Villegas *et al.*[15] executed numerical simulations to examine the shape and spreading behavior of a droplet during the Leidenfrost state, for different Weber numbers ($We = \frac{\rho U^2 D_o}{\sigma}$, represents the ratio of inertial force to surface tension force) and validated with experimental observations. They have also explained the influence of loss of momentum due to viscous dissipation inside the droplet on the droplet shape evolution and the satellite droplet formation.[15] Qiao *et al.* performed numerical simulations of the Leidenfrost droplet (using the lattice Boltzmann method) on liquid pools and reported the role of different non-dimensional numbers such as Stefan number (is defined as the ratio of sensible heat to latent heat), Bond number (described as the ratio of gravitational force to capillary force), and Ohnesorge number (is defined as the ratio of viscous forces to inertial-capillary forces), pool depth and impact height on droplet impact hydrodynamics. They have also numerically examined and reported the role of Stefan flow on the generation of strong airflow between the drop and the heated pool during the Leidenfrost state.[16]

Ulahannan *et al.*[17] studied the effect of the shape of nanoparticles on the shift of the Leidenfrost point. In comparison to de-ionized (DI) water, they reported a decrease in Leidenfrost point for an aqueous solution of both spherical and cylindrical Al_2O_3 nanoparticles. Further, experimental studies have also highlighted the role of surface roughness on the modulation of the Leidenfrost point, by providing different geometries of the various microstructures[18–20] with different surface engineering techniques, viz., polished, particle blasted, porous ceramics,[21] particle coated[22] and rough sanded surface finish.[23] Along a different approach, Biance *et al.* examined and reported the effect of droplet size and shape on the stability of the vapor layer formation during the Leidenfrost state.[24] Tran *et al.* showed the scaling analysis for the maximum spreading of the impacting droplet on both hydrophilic and hydrophobic heated surfaces, and distinguished the different boiling regimes as contact boiling, gentle, and spray film boiling.[25] Next, Khavari *et al.* experimentally examined and segregated the different boiling regimes as spreading regime, bubbly boiling, fingering boiling, and Leidenfrost regime based on the various fingering patterns of the droplet during the Leidenfrost regime.[26]

Nanocolloids have great potential for the efficiency of cooling in various thermal engineering applications, such as emergent core cooling of nuclear reactors in a nuclear powerplant, electronics cooling, and material quenching, etc. The enhanced thermal properties of nanocolloids play a vital role in thermal management systems[27,28] and in spray cooling and drop-wise cooling applications.[29–31] Some of the earlier studies have reported various mechanisms on the shift of T_{DL} with different kinds of fluids like polymers, surfactants, and nanobubbles.[9–13] Though previous studies[8,17] have examined the effect of the size and shape of nanoparticles on the Leidenfrost temperature a clear insight into the mechanism responsible for the change in T_{DL} with nanocolloidal droplets is still lacking. In this present article, we mainly focus on understanding the impact of thermo-hydrodynamic behavior of the nanocolloidal droplets during dynamic Leidenfrost state with different *We* ranging from 10 to 168 in detail and targeted to delay the Leidenfrost regime.

II. MATERIALS AND METHODS

A schematic of the experimental setup used in this study is illustrated in Fig. 1. We used a smooth polished square ($180 \times 180\,mm^2$) stainless-steel plate, mounted over heating coils, as a hot substrate (Holmarc Opto-Mechatronics Ltd., India). Similar to our previous studies,[12,13] substrate temperatures ranging from 150 to 400 °C wwer-ealtered by using a digitized temperature controller. A T-type thermocouple was installed into the substrate and was used to measure and control the temperature at ∼1 mm below that of the top surface (where drop impacts). The temperature controller maintained the substrate at near isothermal conditions (±2–3 °C deviations) from the set temperature point. In order to change the *We* ($We = \frac{\rho U^2 D_o}{\sigma}$, where ρ, U, D_o, and σ represents the density, impact velocity, pre-impact droplet diameter, and surface the ension, respectively), we altered the impact velocity ($U = \sqrt{2\,gH}$), where g and H denote acceleration due to gravity and the droplet release height t from the targeted heated substrate. The release height of the droplet was changed by a droplet dispenser with a digitized controller.[32] A microliter syringe (± 0.1 μl volumetric accuracy) attached to the droplet dispenser was utilized to dispense the droplets of required volume through a flat head steel needle (22 gauge). A high-speed camera (Fastcam Mini-100, Photron, UK) was utilized to capture the hydrodynamic events of the Leidenfrost phenomenon. All the experiments were recorded using a macrolens (Nikon) of 105 mm focal length by maintaining 4000 frames per second and 1024 × 1024 resolution with a spatial resolution of 8.47 μm per pixel and shutter minimum exposure time of 2.7 μs.

Before carrying out each experiment, we cleaned the test substrate with acetone to remove dirt and contaminants from the surface. In this present study, we used colloidal dispersions of aluminum oxide (Al_2O_3) nanoparticles (Alfa Aesar India, > 98.5% purity, average particle size of 20–30 nm) in de-ionized (DI) water as the test fluids. To prepare nanocolloids, we dispersed different weight percentages of nanoparticles ranging from 0.1% to 1% into water. As earlier reported,[33] the nanofluids were mechanically stirred for 30 min and further subjected to ultra-sonication for 2 h to disrupt the agglomeration of nanoparticles. The synthesized colloids were observed to be stable for over 24–36 h, which surpasses the experimental timescales by a large margin. We adopt the pendant drop method to measure the surface tension of the nanocolloidal droplets. We have conducted a rheological flow curve test with parallel plate geometry (PP-20) to determine the shear viscosity of nanocolloidal solutions. Similarly, we measured both $(D_r)_{max}$ and D_o through image processing by using

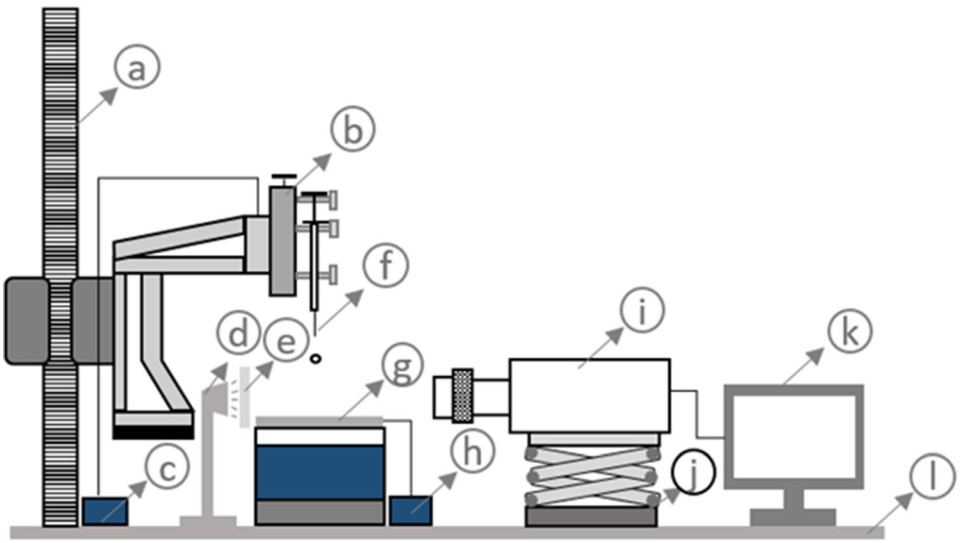

FIG. 1. Schematic of the experimental setup: (a) motorized xyz stage, (b) droplet dispensing mechanism (DDM) unit, (c) DDM controller, (d) strobe light, (e) diffuser, (f) microliter syringe, (g) hot substrate, (h) hot substrate controller, (i) high speed camera, (j) Micron Lab jack, (k) computer for data acquisition and camera control, and (l) vibration isolation table top.

ImageJ software. All thermophysical properties of nanocolloids have been tabulated in Table I.

III. RESULTS AND DISCUSSION

In this section, we discussed the impact dynamics of the nanocolloidal droplets for different *We* and for different substrate temperatures (150–400 °C). The minimum temperature at which the droplet showed rebound behavior for the first time, with minimal spraying was considered the dynamic Leidenfrost temperature (T_{DL}). The corresponding boiling state is defined as the rebounding Leidenfrost state and residue-rebounding Leidenfrost state for water and nanocolloidal droplets, respectively.

A. Transformation of contact boiling in nanocolloidal droplets ($T_S \sim 150\,^{\circ}C < T_{DL}$)

At the lower end of the substrate temperatures tested ($T_S \sim 150\,^{\circ}C$), the contact boiling stage was observed along with residue formation from the nanocolloidal droplets. Figure 2 (Multimedia views) illustrates the temporal evolutions of the nanocolloidal droplets during the contact boiling ($T_S \sim 150\,^{\circ}C < T_{DL}$) regime. Each cell of Fig. 2 represents the side (left part) and top view (right part) at a given instant. Unlike DI water droplets [Fig. 2(a) (Multimedia view)], the nanocolloidal droplets show various transformations in the contact boiling with an increase in contact time. We categorized the transformations such that, where parent nanocolloidal droplet maintains contact with the heated substrate along with secondary droplets spraying termed as spray boiling[34,35] (a yellow color shaded region in Fig. 2). After attainment of the spray boiling regime similar to an earlier reported study,[26] the nanocolloidal droplet also exhibits contact boiling together with a foamy kind of bubble nucleation with an increase in contact time is defined as bubbly boiling[36] (a green color circumscribed region in Fig. 2). The nanoparticles are probably acting as nucleation sites for bubble generation [Figs. 2(b)–2(e) (Multimedia views)]. As a result with an increase in the nanoparticles concentration, the onset of bubbly boiling is observed earlier.

TABLE I. Thermophysical properties of impacting nanocolloidal droplets at 25 °C; pre-impact droplet diameter D_o (mm), density ρ (kg/m^3), surface tension σ (mN/m), viscosity η (mPa s).

Liquid/particles		D_o	ρ	σ	η
DI water		2.64	995.67	71.03	0.791
Al_2O_3	0.1%(w/w)	2.78	997.97	70.8	0.806
	0.5%(w/w)	2.81	1009.87	70.26	0.807
	0.75%(w/w)	2.89	1017.3	69.84	0.806
	1%(w/w)	2.96	1024.75	69.7	0.807

With the furthermore increase in contact time, the contact boiling regime of nanocolloidal droplets left a thin residue desk over the hot surface before complete evaporation of liquid. This stage is described as the residue deposition stage. The diffusion of the nanoparticles also plays a vital role in residue formation and affects the amount of residue left on the hot surface before evaporation.[37] Figure 2 (see even columns) shows the size of residue changes with nanoparticle concentration. Such residue formation was not observed in the case of water droplets (Fig. 2, first row, 11–12th columns). With an increase in the concentration of nanoparticles, the boiling period decreased. Consequently, the disk containing the nanoparticles also deposits sooner may be due to the more conduction from the residue disk to the liquid. For instance, the 1%w/w nanoparticle concentration forms residue on the heated substrate at 679.5 ms at a fixed *We* ~10. However, at the same *We*, low nanoparticle concentration (0.1%w/w) deposits residue on the heated substrate at 1018 ms.

Figure 3 represents the variation of non-dimensionalized residue disk $D^* = (D_r)_{max}/D_o$; where $(D_r)_{max}, D_o$ denotes the maximum diameter of the residue disk on the heated substrate and pre-impact droplet diameter, respectively. We have considered the residue diameter (D_r) of nanocolloidal droplet as the diameter of the thin residue disk left over the hot substrate after complete evaporation of the liquid droplet. The residue resembling a thin disk increased in size with an increase in nanoparticle concentration at a fixed *We* (Fig. 3) due to the

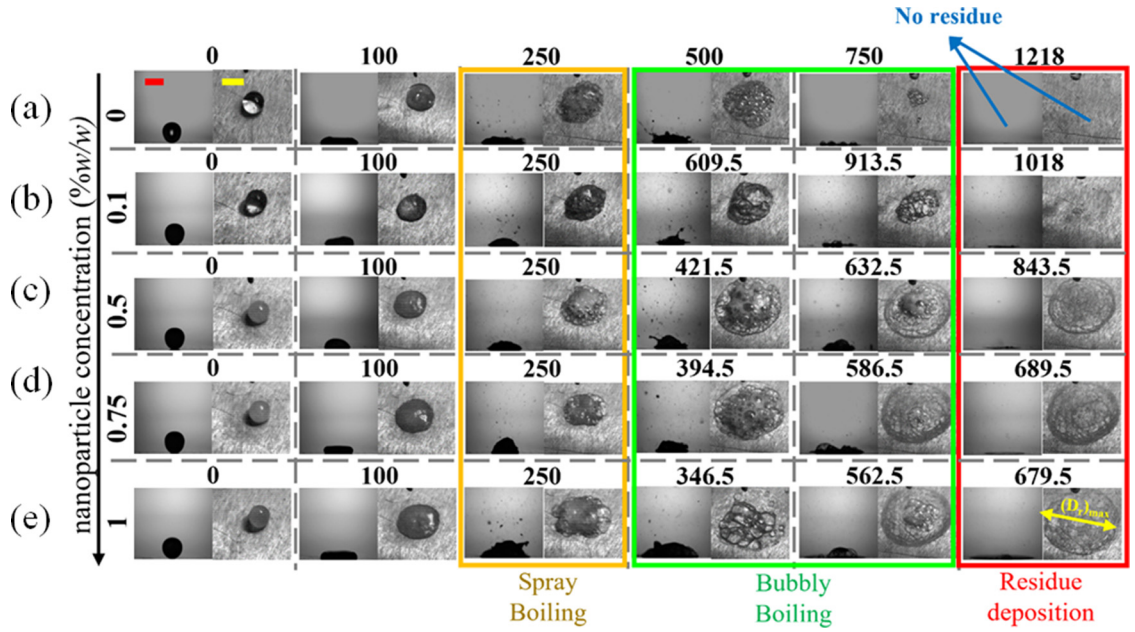

FIG. 2. Various transformations of contact boiling in nanocolloidal droplets at *We* ~10 at ($T_S \sim 150\,^{\circ}C$). The working fluids are (a) water; (b) 0.1% (w/w); (c) 0.5% (w/w); (d) 0.75% (w/w); and (e) 1% (w/w). In the array matrix (represented with gray color dashed lines), the cluster of two images represents the side view (left side image) and top view (right side image). The timeframe numbers (0, 100, 250, 500, 750, and 1012) above each cluster are in ms (milliseconds). The scale bar in the top-left corner of the first (side-view) and second (top view) columns represent 2.96 mm. Spray boiling, bubbly boiling, and residue deposition stage are represented by yellow, green, and red color-shaded regions, respectively. Top view movies of each concentration are provided for further clarity: water (a); 0.1% (w/w) (b); 0.5% (w/w); (c) 0.75% (w/w) (d); and 1%(w/w) (e). Multimedia views: https://doi.org/10.1063/5.0131609.1; https://doi.org/10.1063/5.0131609.2; https://doi.org/10.1063/5.0131609.3; https://doi.org/10.1063/5.0131609.4; https://doi.org/10.1063/5.0131609.5

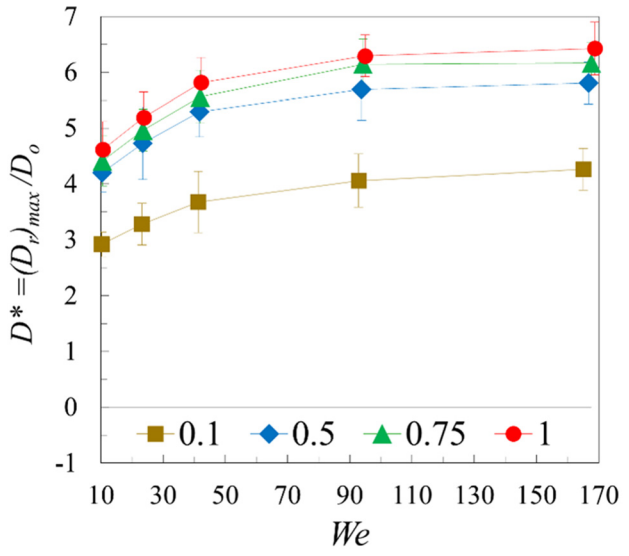

FIG. 3. Variation of non-dimensional residue diameter (D∗) of different concentrations of nanocolloidal droplets over different *We* at ($T_S \sim 150\,^{\circ}C$). The legend values represent the %w/w concentration of nanoparticles of nanocolloids.

more robust bubbly and foaming kind of behavior (see 7–10th columns of Fig. 2). Similarly, it is also noticed that for a particular nanoparticle concentration, the D^* increases with an increase in *We* due to higher impact momentum of the droplet.

B. Role of nanoparticle concentration on T_{DL}

Figure 4(a) shows the temporal evolution of nanocolloidal droplets of varying concentrations at their corresponding T_{DL}. In Fig. 4(a), unlike water droplets, it was observed that the onset of the Leidenfrost phenomenon was accompanied by the minimal spraying of secondary droplets. We presented the effect of nanoparticle concentration on T_{DL} in Fig. 4(b) and observed that T_{DL} increases with an increase in nanoparticle concentration at a particular *We*. Furthermore, it is also noted that the onset of T_{DL} decreases with the rise in *We* for the same nanoparticle concentration. We performed experiments with a temperature difference of 5 °C. To ensure the repeatability of the experiments, we have provided the vertical error bars on the main T_{DL} data point in Fig. 4(b).

Based on earlier studies,[8,38] we noticed that the residue deposition on the heated surface during the spreading stage of the nanocolloidal droplet affects the retraction and bouncing behavior of the droplet. The deposited thin residue disk morphs the heated substrate roughness and enhances the generation of bubble nucleation sites. Although

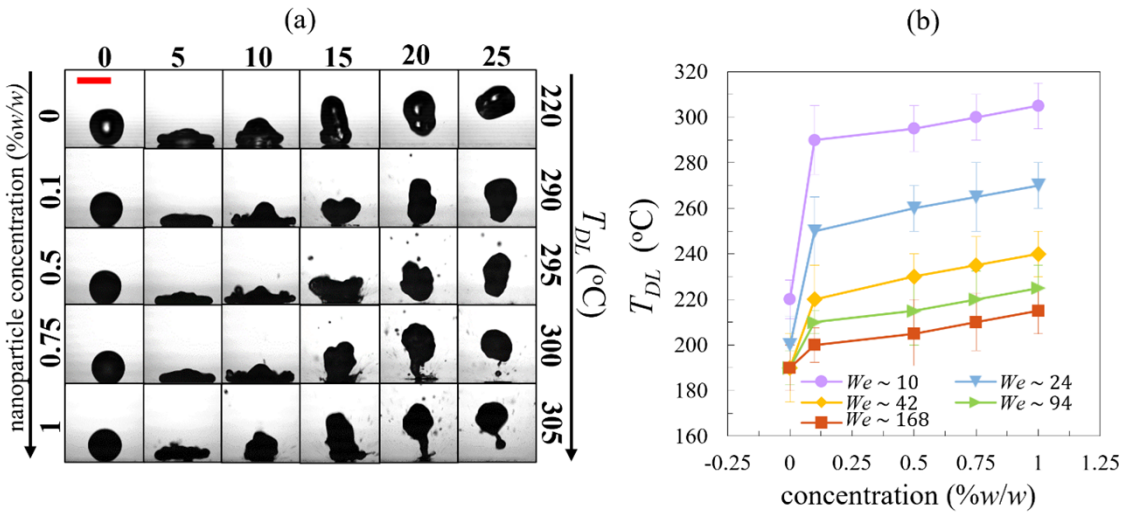

FIG. 4. (a) Temporal evolutions of the side-views of impacting nanocolloidal droplets with low *We* ~10 at their respective T_{DL}'s. All timeframe numbers (0, 5, 10, 15, 20, and 25) above each image in (a) are in ms (milliseconds). (b) Change in the T_{DL} over nanoparticle concentration ranging from 0.1% w/w to 1% w/w for different impact velocities. The scale bar represents 2.96 mm.

the diffusion of nanoparticles plays a crucial role in the shape, thickness, and amount of residue disk left on the heated substrate, we believe that the additional provision of nucleation sites beneath the droplet due to the residue left on the heated substrate play more dominant role on the bubble coalescence. On the one hand, the hot surface wettability greatly alters due to the deposition of the residue beneath the droplet during the spreading stage. It strongly influences the bubble formation, number of bubble nucleation sites, bubble growth, and detachment behavior of vapor bubbles. It consequently affects the retraction and rebounding behavior of nanocolloidal droplets during the Leidenfrost regime. On the other hand, the critical bubble radius and critical distance between two nucleation sites also affect the bubble coalescence behavior.[8,38] From earlier works,[8,38] it was noticed that the bubble departure diameter is below half of the threshold nucleation sites gap, it is difficult for bubbles to coalesce to form a stable vapor layer. Thus, a higher substrate temperature is required to accelerate more vapor bubbles to achieve the Leidenfrost state. Apart from that, the generation of the nucleation sites beneath the droplet also depends on the nanoparticle concentration and its diffusive nature. From Fig. 4(a), the thin residue left on the heated substrate during the spreading state strongly affects the retraction behavior of nanocolloidal droplets by forming more nucleation sites beneath the droplet with an increase in nanoparticle concentration. We believe that the departure diameter of the vapor bubbles from the residue becomes smaller than half of the critical nucleation site gap with an increase in nanoparticle concentration. If the departure diameter of vapor bubbles from residue nucleation sites during retraction is less than the threshold nucleation site gap, it will prevent bubbles coalescence and not support the formation of a stable vapor layer due to Taylor instability.[8] Therefore, a higher surface temperature is required to promote bubble coalescence and generate more nucleation sites for the formation of a stable vapor layer. Hence, T_{DL} was delayed with increasing nanoparticle concentration at constant *We*.

C. Role of Weber number (*We*) on T_{DL}

Next, in this section, the role of *We* on the T_{DL} of nanocolloidal droplets is discussed in detail. Figure 5(a) shows the temporal evolutions of the nanocolloidal droplets of 1% w/w nanoparticle concentration with different *We* at their respective T_{DL}s. It is observed from Fig. 5(a) that the nanocolloidal droplet undergoes vigorous spraying during the onset of the Leidenfrost regime. When nanocolloidal droplet impacts with low impact momentum, the droplet bounces off the surface with very minimal splashing [see the first row of Fig. 5(a)], but in the higher impact momentum case, the parent droplet bounces off with vigorous spraying and secondary droplet atomization [see the fifth row of Fig. 5(a)]. From Fig. 5(a), it was noticed that the spreading diameter of the liquid droplet increases with impact momentum (impact velocity) and leads to form of a larger residue disk beneath the nanocolloidal droplet. The significant increment in the nucleation sites beneath the droplet during retraction promotes a higher rate of bubble coalescence and quicker vapor layer formation relatively at lower substrate temperatures.[39]

Furthermore, we depicted the role of impact *We* on the T_{DL} in Fig. 5(b). From Fig. 5(b), it is noted that the T_{DL} decreases with an increase in impact *We* for a particular nanoparticle concentration. This decreasing trend of T_{DL} with increasing *We* was similar to the Leidenfrost studies with other aqueous solutions of polymers, surfactants, and nanobubbles.[10,12,13] In Fig. 5(b), we have provided the vertical error bars on the main data point to ensure the repeatability of the experiments. The propensity of the generation of more nucleation sites may be increased due to the larger size of the residue disk with an increase in *We*. Hence, we theorize that the increment in the nucleation sites leads to enhance the probability of the bubble coalescence and form a stable vapor sheet relatively at low substrate temperatures due to larger residue disk formation. Thus, T_{DL} decreases with an increase in *We* for a particular nanoparticle concentration. With the aid of scaling analysis, the effect of T_{DL} with impact *We* yield $T_{DL} \sim We^{-0.125}$.

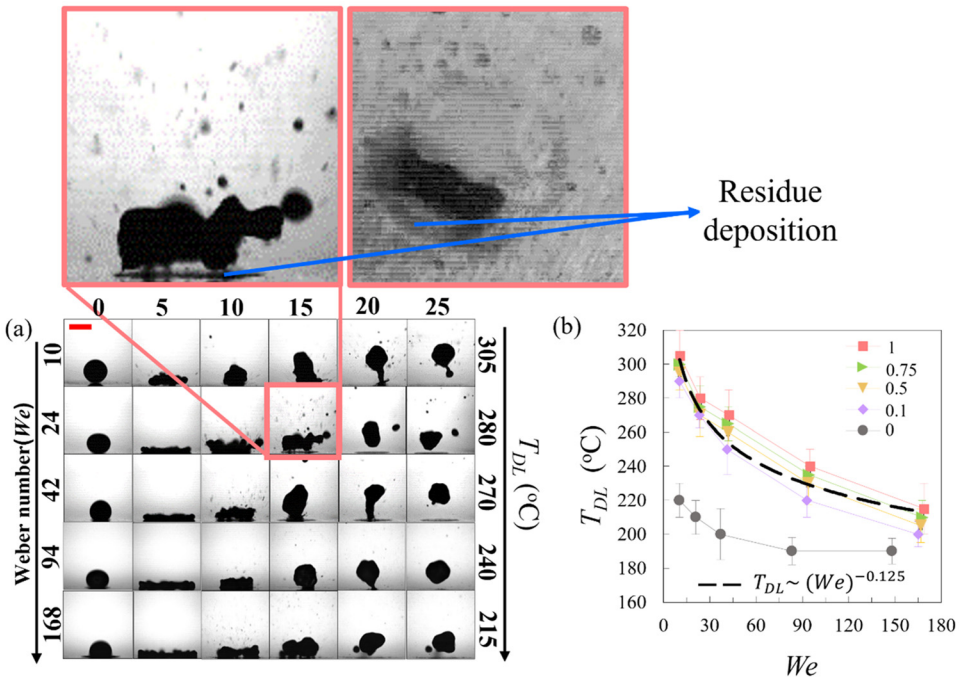

FIG. 5. (a) Temporal evolutions of the side-views of impacting nanocolloidal droplets with 1% w/w nanoparticle concentration at their respective T_{DL}'s. (b) Change in the T_{DL} over different *We* with the variation of nanoparticles concentration. In Fig. 4(b), all legend values were represented as %w/w. All timeframe numbers (0, 5, 10, 15, 20, and 25) above each image in (a) are in ms (milliseconds). The above zoomed version of a side view and top view snapshots evident the residue deposition during levitation of parent nanocolloidal droplet at their respective (T_{DL}). The scale bar represents 2.96 mm.

D. Scaling correlation of T_{DL} with governing Weber number (*We*) and Ohnesorge number (*Oh*)

From the earlier Subsection III C, it has been revealed that change in the T_{DL} with *We* as follows $T_{DL} \sim We^{-0.125}$. In this section, we tried to develop the scaling correlation with two governing parameters Weber number and Ohnesorge number over experimental T_{DL} values with the minimum possible error band through the least squares regression method. Along with the dominance of inertial and surface tension forces (We = inertial force/interfacial force), it is also essential to consider another non-dimensional number called the Ohnesorge number ($Oh = \frac{\mu}{\sqrt{(\rho\sigma D)}} = \frac{\sqrt{We}}{Re}$), reflects the mutual dominance of viscous and inertial-capillary forces of nanocolloids. We tried to fit the experimental results of T_{DL} in terms of *We* and *Oh* with the minimum possible confidence interval yields the following relationship: $T_{DL} = (aWe^{-b} + c)Oh^{d}$. Through least squares regression, we proposed the scaling correlation of T_{DL} in terms of *We* (almost with $\pm 20\%$ error band, refer to Fig. 6) is reflected as $T_{DL} = (407.5We^{-0.125} + 13600)Oh^{0.6}$. We believe that this developed correlation helps future researchers in this field.

E. Boiling regimes of colloidal nanoparticle fluid droplets

In this section, we present the different boiling regimes[40] of nanocolloidal droplets at various impact *We* in Fig. 7. The segregated boiling regimes were named as contact boiling (C), spray boiling (S), rebounding Leidenfrost (R), residue-rebounding Leidenfrost (RR), and fragmenting boiling (F), respectively. Contrary to the DI water droplets, spray boiling and, residue-rebounding Leidenfrost (RR) behaviors have been exhibited during the droplet impact of nanocolloidal droplets on hot surface. Unlike in DI water droplet case, the nanocolloidal droplet regime phase map shows the rebounding Leidenfrost regime with residue deposition (see yellow color shaded regime area) has been suppressed and compensated with contact boiling and spray

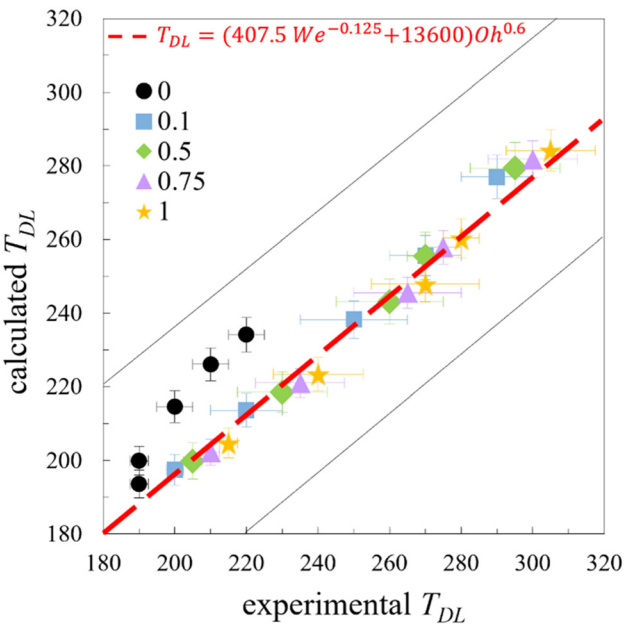

FIG. 6. Fitting of scaling correlation (calculated T_{DL}) over experimental T_{DL} of various concentrations of the nanocolloids. The legend values represent %*w/w* concentration of nanoparticles of nanocolloids. Error bars represents the fluctuation of T_{DL} data point due to repeatability of the experiments.

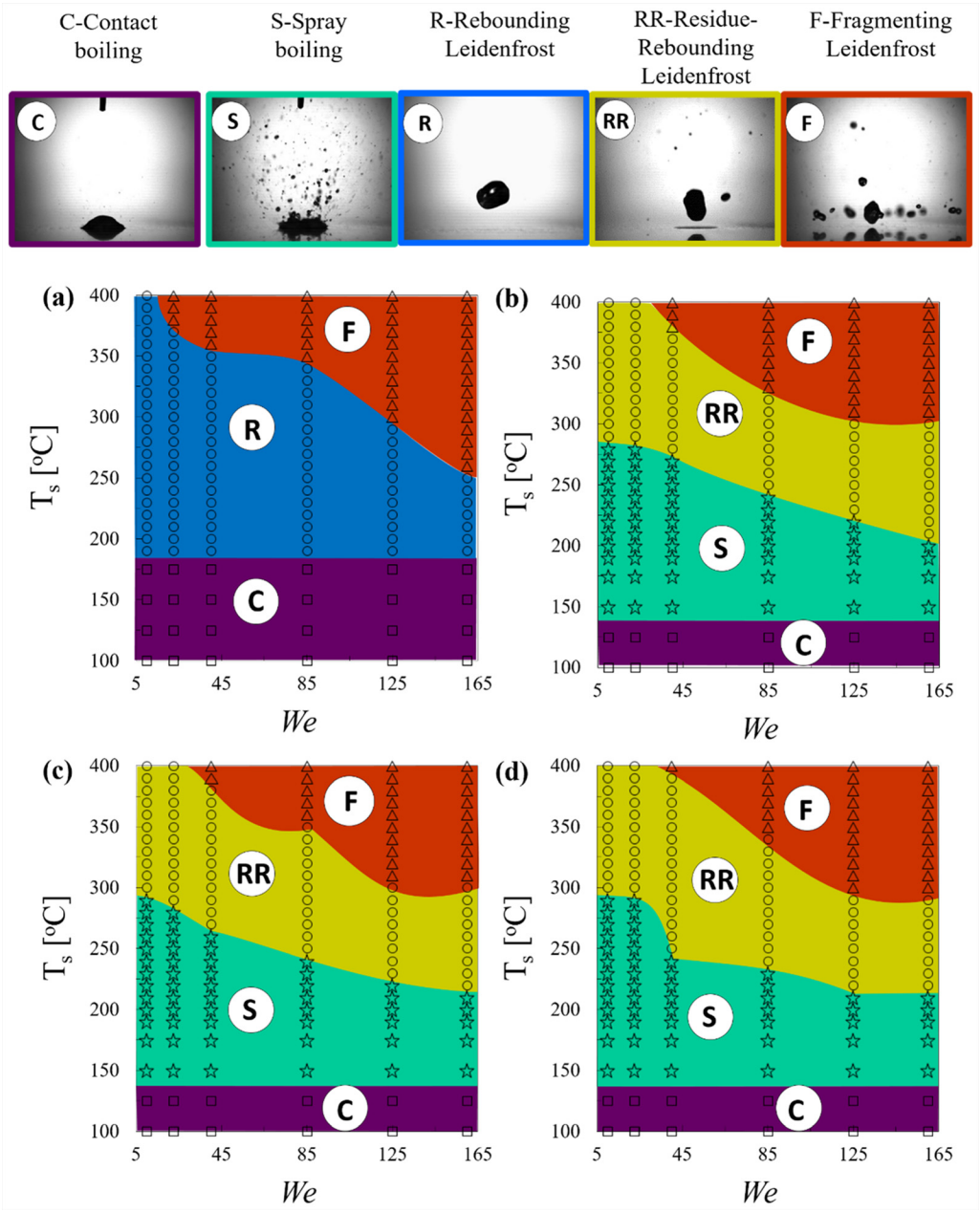

FIG. 7. Various boiling regimes of impacting nanocolloidal droplets with varied *We* of (a) de-ionized water (b)–(d) shows nanocolloidal droplets with the concentration of 0.1%, 0.5%, and1% w/w, respectively. The top row shows paradigmatic images of the different boiling behaviors: C: contact boiling, S: spray boiling, R: rebounding Leidenfrost, RR: residue-rebounding Leidenfrost boiling, and F: fragmenting Leidenfrost.

boiling. Compared to DI water droplets, the addition of nanoparticles lead to increase the T_{DL} as high as 70 °C at a particular $We \sim 10$. Inspite of pure rebound behavior, both spray boiling (see green color shaded region) and residue-rebounding Leidenfrost boiling regimes trigger more with an increase in impact *We* of nanocolloids for a specific concentration of 1% w/w and results in suppressing the rebounding Leidenfrost boiling behavior. Vigorous spraying of nanocolloids attains Leidenfrost state relatively at higher temperatures than DI water droplets at a fixed *We*. Although both rebounding Leidenfrost and residue-rebounding Leidenfrost behaviors are qualitatively different, in the end, they fall into the same Leidenfrost (rebound of parent droplet maybe with an additional residue deposition) state. In this context, it is imperative to discuss the mutual dominance of residue-rebounding Leidenfrost regime and fragmenting Leidenfrost regime in

nanocolloidal droplets against different impact *We*. Unlike the DI water droplet case, the nanocolloidal droplets residue-rebounding Leidenfrost regime transform into fragmenting Leidenfrost regime relatively at higher substrate temperatures at a fixed $We \sim 160$ due to the lack of retraction surface energy against stored impact energy. Thus, finally, from Fig. 7, we emphasize that the overall Leidenfrost (rebounding) regime is suppressed and compensated by spray boiling with an increase in nanoparticle concentration for a fixed *We* and the Leidenfrost (rebounding) regime shrinks more (see yellow colored shaded area) with a rise in impact *We*.

IV. CONCLUSIONS

In summary, we have shown that nanoparticles can be effective in enhancing the T_{DL}. We have shown the onset of residue deposition of nanocolloidal droplets and their vigorous spraying behavior during the contact boiling stage. Next, we reported the role of residue deposition on both bubble coalescence and vapor layer formation against Taylor instability during the Leidenfrost regime. Next, we noticed an increment in T_{DL} with an increase in nanoparticle concentration at a fixed *We* and further report the decrement in the T_{DL} with an increase in the impact on *We*. With the aid of scaling analysis, we have also elucidated the role of impact *We* on the T_{DL} and tried to compare the experimental and fitted T_{DL} with the possible least error band. Finally, based on the rebounding nature of the parent nanocolloidal droplet at different substrate temperatures, we demarcated the boiling regimes of the nanocolloidal droplets as contact boiling, spray boiling, rebounding Leidenfrost, residue-rebounding Leidenfrost and fragmenting Leidenfrost. We believe this study will be relevant for researchers using the efficacy of nanocolloids in heat transfer applications.

ACKNOWLEDGMENTS

GVVSVP would like to thank the Ministry of Education, Government of India, for the doctoral scholarship. D.S. would like to thank IIT Ropar for partially funding the work (vide Grant No. 9-246/2016/IITRPR/144). P.D. thanks IIT Kharagpur (vide grant SFI) and Science and Engineering Research Board (SERB) (vide Grant No. SRG/2020/000004) for partially funding the work.

AUTHOR DECLARATIONS

Conflict of Interest

The authors have no conflicts to disclose.

Author Contributions

Gudlavalleti V V S Vara Prasad: Data curation (equal); Formal analysis (equal); Investigation (equal); Writing – original draft (equal). **Mohit Yadav:** Data curation (equal); Formal analysis (equal); Investigation (equal). **Purbarun Dhar:** Conceptualization (equal); Funding acquisition (equal); Investigation (equal); Project administration (equal); Resources (equal); Writing – review & editing (equal). **Devranjan Samanta:** Conceptualization (equal); Formal analysis (equal); Funding acquisition (equal); Investigation (equal); Methodology (equal); Project administration (equal); Resources (equal); Supervision (equal); Writing – review & editing (equal).

DATA AVAILABILITY

The data that support the findings of this study are available from the corresponding author upon reasonable request.

REFERENCES

[1]J. G. Leidenfrost, *De Aquae Communis Nonnullis Qualitatibus Tractatus* (Ovenius, 1756).
[2]J. Kim, "Spray cooling heat transfer: The state of the art," Int. J. Heat Fluid Flow **28**(4), 753–767 (2007).
[3]G. Grant, J. Brenton, and D. Drysdale, "Fire suppression by water sprays," Prog. Energy Combust. Sci. **26**(2), 79–130 (2000).
[4]S. V. Garimella *et al.*, "Thermal challenges in next-generation electronic systems," IEEE Trans. Compon. Package Technol. **31**(4), 801–815 (2008).
[5]B. Liščić, "Heat transfer control during quenching," Mater. Manuf. Process **24**(7–8), 879–886 (2009).
[6]H. van Dam, "Physics of nuclear reactor safety," Rep. Prog. Phys. **55**(11), 2025–2077 (1992).
[7]G. Duursma, K. Sefiane, and A. Kennedy, "Experimental studies of nanofluid droplets in spray cooling," Heat Transfer Eng. **30**(13), 1108–1120 (2009).
[8]G. Paul, P. K. Das, and I. Manna, "Nanoparticle deposition from nanofluid droplets during Leidenfrost phenomenon and consequent rise in transition temperature," Int. J. Heat Mass Transfer **148**, 119110 (2020).
[9]V. Bertola, "An experimental study of bouncing Leidenfrost drops: Comparison between Newtonian and viscoelastic liquids," Int. J. Heat Mass Transfer **52**(7–8), 1786–1793 (2009).
[10]P. Dhar, S. R. Mishra, A. Gairola, and D. Samanta, "Delayed Leidenfrost phenomenon during impact of elastic fluid droplets: Leidenfrost phenomena," Proc. R. Soc. A Math. Phys. Eng. Sci. **476**(2243), 20200556 (2020).
[11]H. Chen, W.-L. Cheng, Y.-H. Peng, and L.-J. Jiang, "Dynamic Leidenfrost temperature increase of impacting droplets containing high-alcohol surfactant," Int. J. Heat Mass Transfer **118**, 1160–1168 (2018).
[12]G. V. V. S. V. Prasad, P. Dhar, and D. Samanta, "Postponement of dynamic Leidenfrost phenomenon during droplet impact of surfactant solutions," Int. J. Heat Mass Transfer **189**, 122675 (2022).
[13]G. V. V. S. V. Prasad, H. Sharma, N. Nirmalkar, P. Dhar, and D. Samanta, "Augmenting the Leidenfrost temperature of droplets via nanobubble dispersion," Langmuir (published online) (2022).
[14]F. Celestini and G. Kirstetter, "Effect of an electric field on a Leidenfrost droplet," Soft Matter **8**(22), 5992–5995 (2012).
[15]L. Rueda Villegas, S. Tanguy, G. Castanet, O. Caballina, and F. Lemoine, "Direct numerical simulation of the impact of a droplet onto a hot surface above the Leidenfrost temperature," Int. J. Heat Mass Transfer **104**, 1090–1109 (2017).
[16]L. Qiao, Z. Zeng, H. Xie, H. Liu, and L. Zhang, "Modeling Leidenfrost drops over heated liquid substrates," Int. J. Heat Mass Transfer **128**, 1296–1306 (2019).
[17]L. Ulahannan, K. Krishnakumar, A. R. Nair, and S. K. Ranjith, "An experimental study on the effect of nanoparticle shape on the dynamics of Leidenfrost droplet impingement," Exp. Comput. Multiphase Flow **3**(1), 47–58 (2021).
[18]M. Prat, P. Schmitz, and D. Poulikako, "On the effect of surface roughness on the vapor flow under Leidenfrost-levitated droplets," J. Fluids Eng. Trans. ASME **117**(3), 519–525 (1995).
[19]J. D. Bernardin, C. J. Stebbins, and I. Mudawar, "Effects of surface roughness on water droplet impact history and heat transfer regimes," Int. J. Heat Mass Transfer **40**(1), 73–88 (1996).
[20]H. Kim, B. Truong, J. Buongiorno, and L. W. Hu, "On the effect of surface roughness height, wettability, and nanoporosity on Leidenfrost phenomena," Appl. Phys. Lett. **98**(8), 083121 (2011).
[21]C. T. Avedisian and J. Koplik, "Leidenfrost boiling of methanol droplets on hot porous/ceramic surfaces," Int. J. Heat Mass Transfer **30**(2), 379–393 (1987).
[22]D. D. Hall and I. Mudawar, "Predicting the impact of quenching on mechanical properties of complex-shaped aluminum alloy parts," J. Heat Transfer **117**(2), 479–488 (1995).
[23]H. Kim, G. DeWitt, T. McKrell, J. Buongiorno, and L.-W. Hu, "On the quenching of steel and zircaloy spheres in water-based nanofluids with alumina, silica and diamond nanoparticles," Int. J. Multiphase Flow **35**(5), 427–438 (2009).

[24]A. L. Biance, C. Clanet, and D. Quéré, "Leidenfrost drops," Phys. Fluids **15**(6), 1632–1637 (2003).
[25]T. Tran, H. J. J. Staat, A. Prosperetti, C. Sun, and D. Lohse, "Drop impact on superheated surfaces," Phys. Rev. Lett. **108**(3), 036101 (2012).
[26]M. Khavari, C. Sun, D. Lohse, and T. Tran, "Fingering patterns during droplet impact on heated surfaces," Soft Matter **11**(17), 3298–3303 (2015).
[27]L. T. Carmichael, V. Berry, and B. H. Sage, "Thermal conductivity of fluids. Ethane," J. Chem. Eng. Data **8**(3), 281–285 (1963).
[28]S. M. Kwark, R. Kumar, G. Moreno, J. Yoo, and S. M. You, "Pool boiling characteristics of low concentration nanofluids," Int. J. Heat Mass Transfer **53**(5–6), 972–981 (2010).
[29]D. P. Rini, R. H. Chen, and L. C. Chow, "Bubble behavior and nucleate boiling heat transfer in saturated FC-72 spray cooling," J. Heat Transfer **124**(1), 63–72 (2002).
[30]R. H. Chen, L. C. Chow, and J. E. Navedo, "Optimal spray characteristics in water spray cooling," Int. J. Heat Mass Transfer **47**(23), 5095–5099 (2004).
[31]R. H. Chen, L. C. Chow, and J. E. Navedo, "Effects of spray characteristics on critical heat flux in subcooled water spray cooling," Int. J. Heat Mass Transfer **45**(19), 4033–4043 (2002).
[32]G. V. V. S. V. Prasad, P. Dhar, and D. Samanta, "Magneto-elastic effect in non-Newtonian ferrofluid droplets impacting superhydrophobic surfaces," Langmuir **37**(32), 9673–9682 (2021).
[33]A. Katiyar, P. Dhar, T. Nandi, and S. K. Das, "Magnetic field induced augmented thermal conduction phenomenon in magneto-nanocolloids," J. Magn. Magn. Mater. **419**, 588–599 (2016).
[34]S. S. Hsieh, T. C. Fan, and H. H. Tsai, "Spray cooling characteristics of water and R-134a. Part I: Nucleate boiling," Int. J. Heat Mass Transfer **47**(26), 5703–5712 (2004).
[35]J. D. Bernardin and I. Mudawar, "Transition boiling heat transfer of droplet streams and sprays," J. Heat Transfer **129**(11), 1605–1610 (2007)..
[36]M. Khavari and T. Tran, "Universality of oscillating boiling in Leidenfrost transition," Phys. Rev. E **96**(4), 043102 (2017).
[37]I. Iavicoli, L. Fontana, and G. Nordberg, "The effects of nanoparticles on the renal system," Crit. Rev. Toxicol. **46**(6), 490–560 (2016).
[38]H. M. Kwon, J. C. Bird, and K. K. Varanasi, "Increasing Leidenfrost point using micro-nano hierarchical surface structures," Appl. Phys. Lett. **103**(20), 201601 (2013).
[39]N. Basu, G. R. Warrier, and V. K. Dhir, "Onset of nucleate boiling and active nucleation site density during subcooled flow boiling," J. Heat Transfer **124**(4), 717–728 (2002).
[40]J. D. Bernardin, C. J. Stebbins, and I. Mudawar, "Mapping of impact and heat transfer regimes of water drops impinging on a polished surface," Int. J. Heat Mass Transfer **40**(2), 247–267 (1997).